

Periodic Field Emission from an Isolated Nano-Scale Electron Island

D. V. Scheible¹, C. Weiss², J. P. Kotthaus¹, and R. H. Blick³

¹Center for NanoScience and Fakultät für Physik der Ludwig-Maximilians-Universität,
Geschwister-Scholl-Platz 1, 80539 München, Germany

²Institut für Physik, Carl von Ossietzky Universität, 26111 Oldenburg, Germany

³Department of Electrical & Computer Engineering, University of Wisconsin-Madison, 1415 Engineering Drive, Madison, Wisconsin 53706

(Dated: September 10, 2003)

We observe field emission from an isolated nano-machined gold island. The island is able to mechanically oscillate between two facing electrodes, which provide recharging and detection of the emission current. We are able to trace and reproduce the transition from current flow through a rectangular tunneling barrier to the regime of field emission. A theoretical model via a master-equation reproduces the experimental data and shows deviation from the Fowler-Nordheim description due to the island's electric isolation.

PACS numbers: 73.23.-b, 79.70.+q, 85.45.-w, 87.80.Mj

Field emission by microscopic tips has been a fundamental tool of experimental physics for decades. Deposited thorium at the end of a tungsten tip, acting as a field emitter, provided the first experimental visualization of single atoms [1]. Today, field emission from nano-scale emitters is subject to intense experimental and theoretical research [2, 3, 4, 5, 6, 7]. Bonard *et al.* have studied the emission from individual carbon nanotubes [2], where deviation from the classical description of field emission by Fowler and Nordheim (FN) [8] is caused by geometrical effects and the particular electronic structure of the nanotubes [3, 4]. Purcell *et al.* have observed field emission from single nanotubes whilst the tubes were excited resonantly in one of their mechanical eigenmodes [9]. In this Letter, we demonstrate field emission from an *isolated* nano-scale entity: a gold island is brought mechanically into an electric field configuration which provides the local field strength necessary for field emission. The island oscillates between the point of charge depletion toward one electrode, and the point at which it is recharged from a second electrode at the end of each cycle. Contrary to earlier observed deviation from the FN-formalism, the isolated nanomechanical pendulum shows new behavior already at low voltages. The fact that the emitter is isolated alters the FN-description to a behavior which becomes linear for large voltages.

Hitherto conceived experiments of current spectroscopy in nano-scale electronic systems, such as laterally defined quantum dots [10, 11], mostly work in the regime of electrons tunneling through a barrier which is independent of the source-drain field. The same applies to nano-scale systems achieving electrical current transport across a structure with a mechanical degree of freedom [12, 13]. Mechanical displacement modulates the tunnel barrier and consequently regulates current transport [14] and enables the suppression of co-tunneling [15]. The size of the island in the present device has been reduced six-fold compared to preceding work [12], thus increasing the electric field strength. As a consequence, the device undergoes the transition into the response of field emission and enhances strongly its net current up to several nano-Amperes. In our setup field emission is controlled by both the voltage bias and the mechanical oscillations of the emitter.

Operation of nano-electromechanical systems (NEMS), which have become an integral part of experimental mesoscopic physics [16, 17], is predominantly carried out by the Lorentz force caused by an AC current in a perpendicular magnetic field. This magnetomotive drive requires high magnetic field densities (up to 15 Teslas), and consequently elaborate cryogenic cooling. In contrast to that, we drive our nanomechanical resonator by a combination of the capacitive force and the Coulomb force onto the excess charge being present on the shuttle island [15, 18]. The latter is strongly enhanced in the high current regime via field emission and therefore eases excitation. This mechanical excitation results in an oscillating shuttle between two facing gates, which provide the electric field and allow charging and discharging of the shuttle, when deflected toward the respective gate [19].

Our experimental setup consists of a nano-machined cantilever made from silicon-on-insulator material. At the tip of a freely suspended silicon cantilever of about 1 micron length we deposited an isolated gold island with dimensions $80 \times 80 \times 50 \text{ nm}^3$. This resembles a small clamped bell. Two gates A and B face the grounded cantilever C [see Fig. 1(a)], and the island I oscillates between source S and drain D. AC excitation is applied to gate A, whereas an additional DC bias is imposed via source S. The resulting net current I_D is detected at drain D, and recorded versus AC excitation frequency f with the DC bias V as the parameter. We have presented the manufacturing process of such devices elsewhere [20].

As the bow-like bilayer system (Si/Au) strongly changes its dynamical response upon cooling the device, the AC excitation power P has to be increased in order to maintain a stable current level through the nano-mechanical shuttle. Whereas at room temperature a reasonably low power in the range of $P = -30 \dots -10 \text{ dBm}$ suffices for operation [18, 21], we apply an incident AC power of $P = +8 \text{ dBm}$ at a device temperature of 77 K, at which all experiments were conducted. The resulting voltage drop at the NEMS itself lies between $V_0 = \sqrt{PZ_0}$ for the system possessing a matched impedance $Z_0 = 50\Omega$, and $2V_0$ for infinite impedance. As we estimate the actual impedance above 1 k Ω and power losses of the setup to 3 dB, the AC voltage amplitude will be roughly

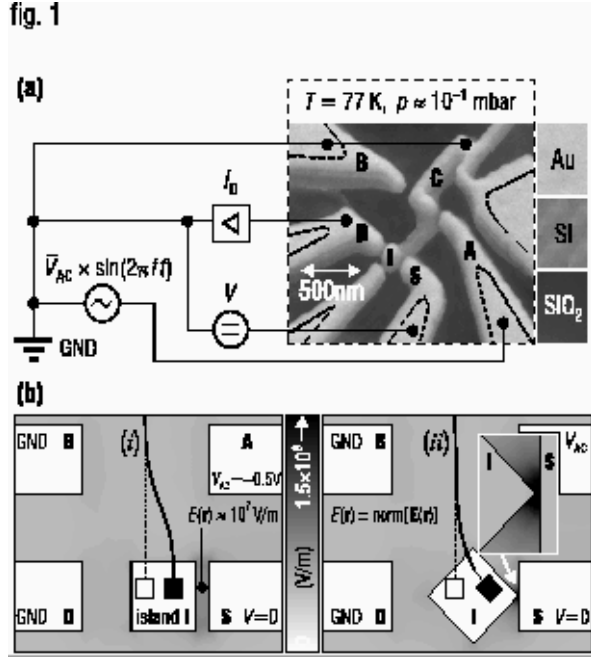


FIG. 1: (a) SEM micrograph and experimental setup of the device: the electron shuttle consists of a gold island I situated at the end of a nano-machined silicon cantilever. Free suspension outside the area marked by the dotted lines is ~ 200 nm above the sacrificial layer (SiO_2). The island oscillates between source S and drain D, where the current I_D is detected via a current amplifier. AC excitation is applied at frequency f at gate A with a voltage amplitude of $\bar{V}_{AC} \approx 500$ mV. The DC bias V is superimposed on gate S. (b) Finite element solution of Maxwell's equations yielding the local electric field strength $|\mathbf{E}(\mathbf{r})|$, ranging from zero (white) to 1.0×10^8 V/m (black) for an instantaneous external bias of $V_{AC} = -500$ mV at gate A, and a neutral island charge ($n_I = 0$). In (i) the shuttle is deflected parallel toward drain, whereas in (ii) the same deflection of the center of mass is assumed with an edge facing the gate. The inset magnifies the facing tip with the absolute field maximum of 6.9×10^9 V/m. This explains the manifestation of field emission only for specific modes of excitation.

$\bar{V}_{AC} \approx 500$ mV. This amplitude allows the NEMS to establish the transition from tunneling to field emission. The small gate-island distance of some tens of nanometers and local microscopic surface roughness, induced by the dry reactive ion etching [6], support the manifestation of field emission.

Single electron devices with a mechanical degree of freedom are well modelled by a master equation, describing the time dependence of the number of electrons on the oscillating island [14, 15]:

$$\begin{aligned} \dot{p}(m,t) = & -[\Gamma_L^+(m,t) + \Gamma_R^+(m,t)] p(m,t) \\ & -[\Gamma_L^-(m,t) + \Gamma_R^-(m,t)] p(m,t) \\ & +[\Gamma_L^+(m-1,t) + \Gamma_R^+(m-1,t)] p(m-1,t) \\ & +[\Gamma_L^-(m+1,t) + \Gamma_R^-(m+1,t)] p(m+1,t), \end{aligned} \quad (1)$$

where Γ are the transition rates and p the probability to find m additional electrons on the island at time t . For devices in which charge current is established by tunneling, the golden

rule transition rates are of the form [22]

$$\Gamma_t = \frac{1}{e^2 R} \frac{\Delta E}{1 - \exp(-\Delta E/k_B T)}. \quad (2)$$

This approach was already successfully applied to explain earlier experiments [12] and also reproduces the response of the present device when still in the tunneling regime (see Fig. 2). Since the tunneling rate and therefore the resistance depends exponentially on the distance between gate and island, charge transport takes place only when the island is deflected toward one of the electrodes (co-tunneling can therefore be neglected). In the experimental regime where the field emission behavior is not yet visible, the tunneling time τ is large compared to the effective contact time $\propto 1/f$ [15]: although the applied driving voltage acts as a rather large gate voltage on the island, the effective number n of electrons transferred per period is of the order of $0 < n < 1$.

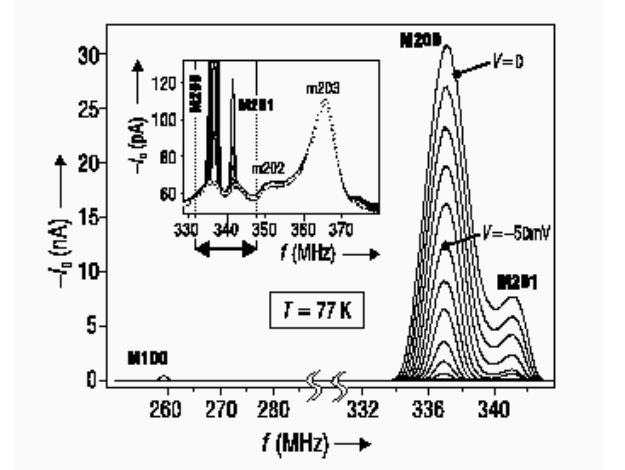


FIG. 2: Spectral drain current $-I_D$ vs excitation frequency f for bands in which field emission occurs first (DC bias V ranges from 0 to -200 mV). These three modes are denoted by M100, M200, and M201. The inset shows the transition from tunneling to field emission in a magnified current scale. The current differs roughly by two orders of magnitude. The dotted line is a tunneling fit for a set of superimposed resonances, according to the standard theory of a single electron shuttle of equations (1) and (2). The arrow corresponds to the respective scope given in the main figure.

For higher driving voltages (and thus larger electric fields between island and electrode), field emission between island and source electrode leads to a strongly positively charged island approaching the drain electrode. This results in a current which is several orders of magnitude larger. Applying a DC source voltage V will either increase the field (for positive voltages) or decrease the field (for negative voltages). In a single tunneling event, the tunneling probability decreases exponentially with distance x as $\exp(-x/\lambda)$ for comparatively low electric fields. This can be seen in the tunneling resistance R of Eq. (2). For field emission this exponential decrease is

replaced [23] by a factor of

$$D = \exp\left[-\frac{A}{\mathcal{E}}\right], \quad A > 0, \quad (3)$$

where the electric field \mathcal{E} in our case can be taken to be proportional to the voltage difference $V + V_0$ between source electrode and island. The parameter A accounts for the material specific emission behavior.

However, even for a stationary pendulum, emission eventually stops as the island gets more and more positively charged. The total number of electrons will scale roughly linear [14, 15] with the applied voltage. Thus, we can assume the number of electrons on the island n_I after field emission (which only takes place for $V + V_0 > 0$) to be proportional to the product of the applied voltage and the transition probability (3), i.e.

$$n_I \propto (V + V_0) \exp\left[-\frac{B}{V + V_0}\right], \quad V + V_0 > 0. \quad (4)$$

Geometrical details of the shuttle, as well as the material constant A , are contained in the parameter $B > 0$. We describe the number of electrons on the island after field emission with Eq. (4) and the tunneling at the other electrode again numerically with equations (1) and (2). This results in a current proportional to the number of electrons on the island given by

$$I = \begin{cases} I_0 \frac{V+V_0}{V_0} \exp\left[-\frac{B}{V+V_0}\right] & : V + V_0 > 0 \\ 0 & : V + V_0 \leq 0 \end{cases}. \quad (5)$$

This equation differs remarkably from ordinary field emission, since the emission takes place from an isolated entity: the I - V -characteristics lead to a linear dependence on the voltage V for $V \gg V_0$, rather than the quadratic behavior predicted by FN-tunneling [8, 23].

Experimental current traces are plotted in Fig. 2. In the main figure only three modes are visible in the high-current scale ranging up to 30 nA. These modes, denoted with a capital 'M' (M100, M200, and M201), show field emission. Magnification of the current axis reveals a second set of resonances which develop a much smaller absolute peak current of the order of only 50 pA (e.g. m202 and m203). This latter data can be fitted well by a set of superimposed resonances, assuming the shuttle transport to lie in the pure tunneling regime of Eq. (2). Hence their denotation by a lower-case 'm'. Furthermore, the response in the tunneling regime does not show dependence on the dc bias V , as already observed and analyzed earlier [12].

If a mode sustains suitable mechanical response, i.e. island deflection toward gates is in a way that surface roughness or device edges result in a sufficiently high electric field strength [see mode (ii) in Fig. 1(b)], transition from tunneling current to the field emission current occurs. As shown in the inset of Fig. 2, some modes ignite (M200, M201) at particular frequencies, based on their respective tunneling current resonance. Adjacent modes however, such as m202 and

m203, do not show field emission transport for the given DC bias. In order to unambiguously attribute the observed behavior to field emission, we have applied a DC bias V in the range of -500 mV... $+500$ mV in addition to the AC power at $P = +8$ dBm. All modes M_j could be entirely detuned by a sufficiently negative DC bias V . With a superimposed DC bias of $V = -200$ mV and below field emission is suppressed, and the device is led back entirely into the tunneling regime. For an increasing voltage V however (up to $+500$ mV), the current of the shown modes continues to rise in the discussed manner. Furthermore, more and more modes ignite and develop field emission response, as a positive bias increases the local field strength of any modal configuration of the island. The field emission offset V_0 here is characteristic for each mode M_j . The observed peak current I_D^{peak} scales linearly with the applied bias V for $V \gg V_0$ as given by Eq. (5). Figure 3 shows good accordance of the experimental values with this analytic fit, and gives evidence for the emission from the isolated shuttle island.

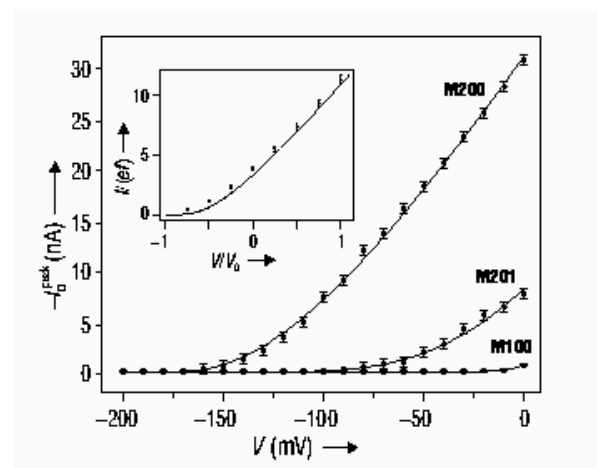


FIG. 3: Peak current I_D^{peak} vs DC bias voltage V for the first three modes which show transition to field emission. Error bars correspond to maximum variation during the averaged recording of the spectral current. The data have been fitted according to Eq. (5). Inset: If n_I electrons are on the island after field emission, a Monte-Carlo integration of the tunneling at the other electrode (points) yields a current $I = gn_I e f$ with $g < 1$ (solid line) and thus justifying the analytic curve Eq. (5). The latter describes well the experimental results.

Although at zero DC bias ($V = 0$) a couple of modes show field emission, the majority of the dynamic response remains well within the tunneling regime. This is caused by the particular deflection of the island for each mode. We have modelled the magnitude of the electric field strength $E(\mathbf{r}) \equiv \text{norm}[\mathbf{E}(\mathbf{r})]$ via a finite element simulation [24] for the two most prominent cases: either the shuttle island faces a gate with the boundaries aligned parallel to each other, or an edge of the island — respectively any other tip of the rough surface — causes field enhancement. Both situations are drawn in Fig. 1(b), and the simulation shows an increase of the maximum field strength up to 6.9×10^9 V/m, which suffices for

field emission [23]. We have to stress that this is solely induced by a changed mode, keeping constant the deflection of the center of mass and the external bias. The finite element calculation assumes perfectly smooth surfaces rather than surface roughness. For the latter case, as it is in the experiment, the field strength is further increased.

The nano-scale configuration of our device allowed the manifestation of field emission already at externally applied voltages below 1 Volt. The emission takes place from the isolated island toward one gate and a periodic oscillation allows recharging and hence quasi-continuous operation. Theoretical calculations, based on this model, well comply with the experimentally obtained data. Deviation from the classical FN-description of field emission can be attributed to the electrical isolation of the emitter. Excitation via the large excess charge on the shuttle was demonstrated and the manifestation of field emission in our NEMS yields a large current enhancement by a factor of $10^2 \dots 10^3$. We consider the combination of the environmentally sensitive field emission with the mechanical degree of freedom of a NEMS very promising for the interaction of the device with bio-molecules [25] and traces of specific chemicals [5]. Furthermore, application as a low-power loss radio-frequency filter appears feasible [26].

Authors would like to thank W. Zwerger and S. Manus for stimulating discussions, and A. Kriele and W. Kurpas for expert technical help. DVS gratefully acknowledges financial support by the Deutsche Forschungsgemeinschaft (DFG) under grant Bl-487 and the University of Wisconsin-Madison.

-
- [1] E. W. Müller, *Z. Physik* **106**, 541 (1937).
 [2] J.-M. Bonard, K. A. Dean, B. F. Coll, and C. Klinke, *Phys. Rev. Lett.* **89**, 197602 (2002).
 [3] A. Buldum and J. P. Lu, *Phys. Rev. Lett.* **91**, 236801 (2003).
 [4] X. Zheng, G.-H. Chen, Z. Li, S. Deng, and N. Xu, *Phys. Rev. Lett.* **92**, 106803 (2004).
 [5] A. Modi, N. Koratkar, E. Lass, B. Wei, and P. M. Ajayan, *Nature (London)* **424**, 171 (2003).
 [6] L. Pescini, A. Tilke, R. H. Blick, H. Lorenz, J. P. Kotthaus, W. Eberhardt, and D. Kern, *Adv. Mater.* **13**, 1780 (2001).
 [7] G. Pirio, P. Legagneux, D. Pribat, K. B. K. Teo, M. Chhowalla, G. A. J. Amaratunga, and W. I. Milne, *Nanotech.* **13**, 1 (2002).
 [8] R. H. Fowler and L. Nordheim, *Proc. Royal Soc. (London) Ser. A* **119**, 173 (1928).
 [9] S. T. Purcell, P. Vincent, C. Journet, and V. T. Binh, *Phys. Rev. Lett.* **89**, 276103 (2002).
 [10] A. W. Holleitner, R. H. Blick, A. K. Hüttel, E. Eberl, and J. P. Kotthaus, *Science* **297**, 70 (2002).
 [11] L. P. Kouwenhoven, C. M. Marcus, P. L. McEuen, S. Tarucha, R. M. Westervelt, and N. S. Wingreen, *NATO ASI Ser. E* **345**, 105 (1997).s
 [12] A. Erbe, C. Weiss, W. Zwerger, and R. H. Blick, *Phys. Rev. Lett.* **87**, 096106 (2001).
 [13] H. Park, J. Park, A. K. L. Lim, E. H. Anderson, A. P. Alivisatos, and P. L. McEuen, *Nature (London)* **407**, 57 (2000).
 [14] L. Y. Gorelik, A. Isacsson, M. V. Voinova, B. Kasemo, R. I. Shekhter, and M. Jonson, *Phys. Rev. Lett.* **80**, 4526 (1998).
 [15] C. Weiss and W. Zwerger, *Europhys. Lett.* **47**, 97 (1999).
 [16] R. H. Blick *et al.*, *J. Phys.: Cond. Mat.* **14**, R905 (2002).
 [17] M. L. Roukes, *Phys. World* **14**, 25 (2001).
 [18] D. V. Scheible and R. H. Blick, *Appl. Phys. Lett.* **84**, 4632 (2004).
 [19] M. T. Tuominen, R. V. Krotkov, and M. L. Breuer, *Phys. Rev. Lett.* **83**, 3025 (1999). P. Benjamin, *The Intellectual Rise in Electricity*, (Appleton, New York, 1895).
 [20] D. V. Scheible, A. Erbe, and R. H. Blick, *New J. Phys.* **4**, 86.1 (2002).
 [21] D. V. Scheible, C. Weiss, and R. H. Blick, *J. Appl. Phys.* **96**, 1757 (2004).
 [22] H. Grabert and M. H. Devoret (Ed.s), *Single Charge Tunneling*, (Plenum, New York, 1992).
 [23] S. Flügge, *Practical Quantum Mechanics*, (Springer, New York, 1994).
 [24] FEMLAB finite element system (v2.3).
 [25] M. Rief, F. Oesterhelt, B. Heymann, and H. E. Gaub, *Science* **275**, 1295 (1997).
 [26] C. T.-C. Nguyen, *IEEE Trans. Microwave Theory Tech.* **47**, 1486 (1999).